Multiple NaNbO₃/Nb₂O₅ Heterostructure Nanotubes: A New Class of Ferroelectric/Semiconductor Nanomaterials

By *Chenglin Yan, Liliya Nikolova, Afshin Dadvand, Catalin Harnagea, Andranik Sarkissian, Dmitrii F. Perepichka,* Dongfeng Xue,* and Federico Rosei**

Multiple hetero-nanostructures are a promising new class of materials due to their multifunctional character and the possibility of effectively coupling different properties.[1–4] Hetero-nanostructure systems,[5–7] while more challenging to synthesize, often offer significant advantages over single-component systems.[4,8,9] For example, Si/SiGe-superlattice nanowires exhibit enhanced thermoelectric performance and high electric conductivity relative to Si nanowires.[8,10] The coupling between ferroelectric and magnetic order parameters in a nanostructured BaTiO₃/CoFe₂O₄ ferroelectromagnet facilitates the interconversion of energies stored in electric and magnetic fields.[11] However, fabrication of hetero-nanostructures, especially multiple heterostructures, from distinct materials is challenging due to the lattice mismatch and the difficulty in balancing two dissimilar growth processes with different microscopic mechanisms and reaction rates.[1,2,12]

Here we focus on multiple heterostructures of ferroelectric/semiconductor nanostructures due to their potential for multifunctional device applications.[13,14] Interfacing ferroelectric and semiconductor materials can lead to novel functionalities that are independent of the individual components and may be tailored to fit a specific application, although realization attempts were so far unsuccessful. To achieve practical devices, a number of hurdles need to be overcome, including the creation of multiple heterojunctions obtaining different combinations of materials and exploring their potential use in devices. Here, we demonstrate major advances on these fronts: multiple NaNbO₃ nanoplates are created inside hollow Nb₂O₅ nanotubes, forming a novel class of multiple ferroelectric (NaNbO₃)/semiconductor (Nb₂O₅) heterostructures (bandgap ∼3.4 eV).[15] Specifically, we found that the NaNbO₃ nanoplates within heterostructure nanotubes exhibit distinct ferroelectric switching due to the presence of the tensile stress at the interface between NaNbO₃ and Nb₂O₅ nanostructures, which facilitates the ferroelectric phase. The semiconductive properties of the host Nb₂O₅ nanotubes allow for switching of electrical conductivity by an external electric field, even though ferroelectric NaNbO₃ nanoplates are attached to the inner surface of nanotubes, showing great potential for the fabrication of memory and other multifunctional ferroelectric/semiconductor devices.

The scientific and technological interest in tubular nanostructures such as silicon,[16] carbon,[17] and other inorganic nanotubes[18–20] stem from their fascinating electronic, mechanical, and chemical properties and their ability to serve as templates for confined growth within the nanotube's hollow. Herein, we employed a nanotube-confined growth strategy for the one-step synthesis of multiple NaNbO₃/Nb₂O₅ heterostructure nanotubes, which were prepared by a thermolysis of Nb peroxo complex precursors ($[Nb(O_2)_4]^{3-}$)[21] combined with (slow) fluoride ion corrosion of Nb foil at 180 °C. The formation process is schematically displayed in Figure 1a. Nb₂O₅ nanotubes are first formed under hydrothermal conditions mostly at stage 1. In stage 2, the nucleation of the NaNbO₃ phase preferentially takes place on the inner surface of the Nb₂O₅ nanotubes to form NaNbO₃ nanocrystallites. Finally, in stage 3 the nanocrystallites of NaNbO₃ evolve into nanoplates inside the Nb₂O₅ nanotubes. As shown in a low-magnification scanning electron microscopy (SEM) image (Fig. 1b), the length of the as-prepared multiple-heterostructure nanotube is up to several tens of micrometers with a diameter in the range of 300–600 nm. The structural characteristics of the as-prepared sample are clearly visible in the transmission electron microscopy (TEM) images in Figure 1c, which show a linear arrangement of NaNbO₃ nanoplates of about

[*] Prof. F. Rosei, Dr. C. Yan, L. Nikolova, A. Dadvand, Dr. C. Harnagea
INRS–EMT, Université du Québec
1650 Boul. Lionel Boulet
J3X 1S2 Varennes, QC (Canada)
E-mail: rosei@emt.inrs.ca

Prof. D. Xue
State Key Laboratory of Fine Chemicals
School of Chemical Engineering
Dalian University of Technology
Dalian 116012 (P. R. China)
E-mail: dfxue@chem.dlut.edu.cn

Prof. D. F. Perepichka, Dr. C. Yan
Department of Chemistry, McGill University
801 Sherbrooke Street West
H3A 2K6 Montréal, QC (Canada)
E-mail: dmitrii.perepichka@mcgill.ca

Dr. A. Sarkissian
Plasmionique Inc.,
1650 Boul. Lionel Boulet
J3X 1S2 Varennes, QC (Canada)

Prof. F. Rosei, Prof. D. F. Perepichka
Centre for Self-Assembled Chemical Structures
McGill University
801 Sherbrooke Street West
H3A 2K6 Montréal, QC (Canada)
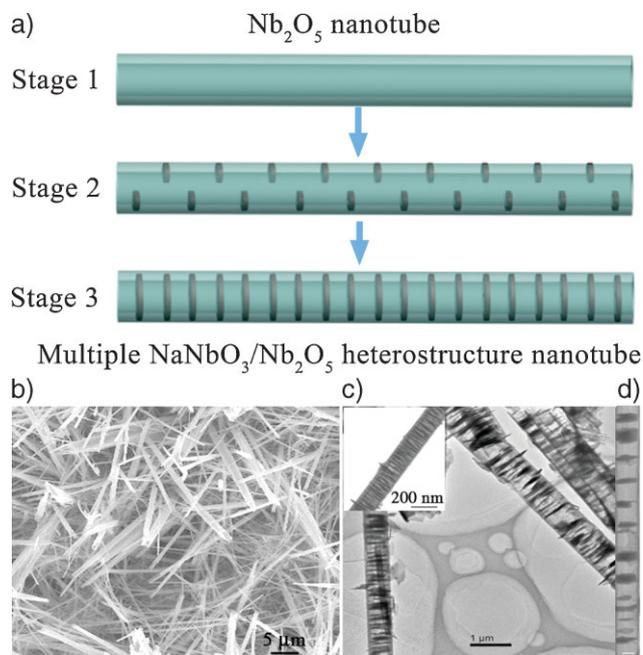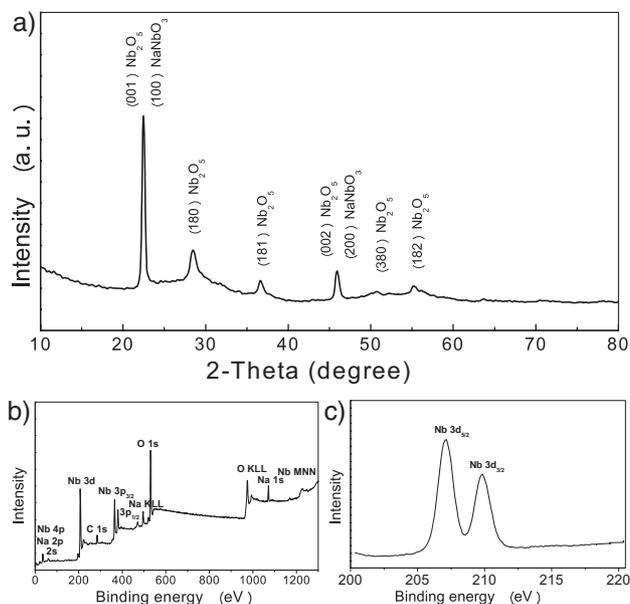
Figure 1. a) Schematic illustration of the formation process of multiple $NaNbO_3/Nb_2O_5$ heterostructure nanotubes. b,c) SEM and TEM images of the as-prepared samples. d) TEM image of a typical heterostructure nanotube (scale bar: 200 nm).
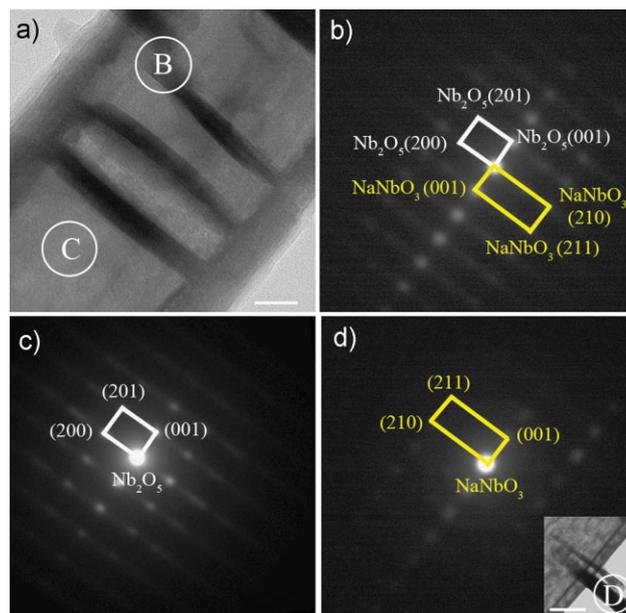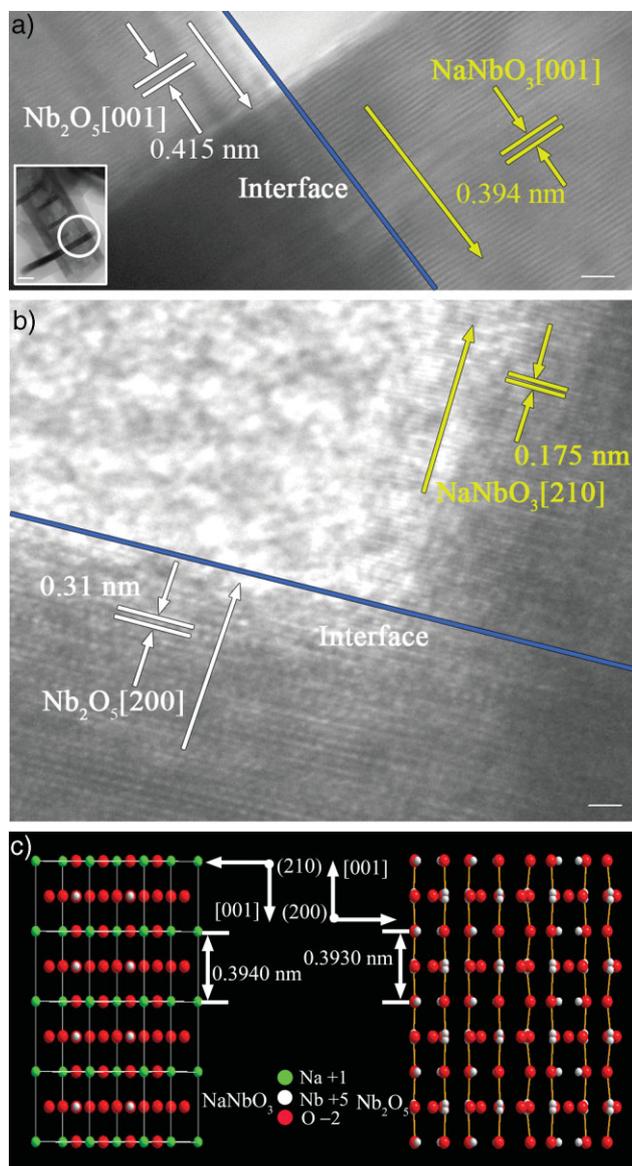

Figure 2. a) XRD pattern of the as-prepared samples. b) XPS spectrum of the as-prepared samples. c) High-resolution XPS spectrum of the Nb 3d core level.

Figure 3. TEM image and SAED patterns of a multiple heterostructure nanotube: a) TEM image of the multiple Nb_2O_5 nanotube and several $NaNbO_3$ nanoplates grown inside the nanotube (scale bar: 20 nm). b) SAED pattern at the interface of Nb_2O_5 and $NaNbO_3$ from the region indicated by white circles in Figure 3a. c) SAED pattern of Nb_2O_5 nanoplates as labeled in Figure 3a. d) SAED pattern of another $NaNbO_3$ nanoplate grown outside the nanotube, the inset shows the corresponding TEM image (scale bar: 30 nm).

20-nm width within the nanotubes. Figure 1d shows that the $NaNbO_3$ nanoplates are perpendicular to the Nb_2O_5 nanotube axes, each of them being sheathed with a uniformly structured Nb_2O_5 shield over its entire length.

X-ray diffraction (XRD) measurements (Fig. 2a) reveal that the as-prepared samples are composed of the orthorhombic phase of Nb_2O_5 with a lattice constants of $a = 0.6175$ nm, $b = 2.917$ nm, and $c = 0.393$ nm (Joint Committee on Powder Diffraction Standards, JCPDS, No. 30-0873) and the pseudocubic perovskite structure[22] of $NaNbO_3$ with a lattice constant of $a = 0.3943$ nm. The peaks near $2\theta = 23°$ and $2\theta = 46°$ correspond to the (001) and (002) planes of the pseudocubic perovskite structure of $NaNbO_3$ (these peaks overlap with the peaks from the Nb_2O_5 nanotubes, making it difficult to ascertain the presence of these species). X-ray photoelectron spectroscopy (XPS) analysis was performed to further identify their chemical composition and valences (Fig. 2b). The typical survey spectrum consists of $Nb3d_{5/2}$ at 210.2 eV and $3d_{3/2}$ at 207.4 eV, O 1s at 529.7 eV, and Na 1s at 1070 eV, confirming the presence of elemental niobium, oxygen, and sodium (Fig. 2b). The high-resolution spectrum for Nb 3d (Fig. 2c) is a simple spin–orbit doublet with a $Nb3d_{5/2}$ binding energy of 210.2 eV, and is consistent with previously observed values[23,24] of $Nb3d_{5/2}$ at 210.2 eV and $3d_{3/2}$ at 207.5 eV for the Nb_2O_5 composition. The XPS results thus prove the elemental composition of these heterostructures, also demonstrating that there is no contamination.

The multiple heterostructure composed of embedded $NaNbO_3$ nanoplates within Nb_2O_5 nanotubes with a wall thickness of around 25 nm (Fig. 3a) is also evidenced from selected area electron diffraction (SAED) patterns, displayed in Figures 3b–c. The dark nanoplate of the nanotube (area B in Fig. 3a) shows two

sets of diffraction patterns corresponding to the (001), (200), and (201) lattice planes of orthorhombic Nb_2O_5 and to the (001), (210), and (211) planes of pseudocubic $NaNbO_3$, (Fig. 3b). However, the lighter part of the nanotube (area C in Fig. 3a) shows a pure

Materials
Views
www.MaterialsViews.com

ADVANCED
MATERIALS
www.advmat.de

COMMUNICATION

Figure 4. a,b) HR-TEM images of two differently oriented heterostructures overlaid with identifications of crystal planes for both NaNbO$_3$ nanoplates and Nb$_2$O$_5$ nanotubes (scale bar: 2 nm), the inset in (a) shows a corresponding TEM image (scale bar: 20 nm). c) Schematic model illustrating the atomic arrangements in the planes of Nb$_2$O$_5$ (001) and NaNbO$_3$ (001), respectively.

Nb$_2$O$_5$ phase in the SAED analysis (Fig. 3c). Also, the SAED pattern of the NaNbO$_3$ nanoplate protruding outside the nanotube shows a pure phase of single crystalline NaNbO$_3$ and no diffraction spots from the Nb$_2$O$_5$ phase. Collectively, these results convincingly show that a unique heterostructure formed inside the Nb$_2$O$_5$ nanotube with occasional NaNbO$_3$ nanoplate outgrowths.

Further high-resolution TEM (HR-TEM) investigations (Fig. 4a) revealed that the marked d-spacings of 0.415 nm and 0.394 nm along the direction parallel to the tube axis match well with both the $d_{(001)}$ interplanar distances of Nb$_2$O$_5$ and NaNbO$_3$, respectively. The dotted line marks the interface between the two

phases along the direction perpendicular to the tube axis (Fig. 4b). The HR-TEM image shows that the marked d-spacings of 0.31 nm and 0.175 nm match well with $d_{(200)}$ of Nb$_2$O$_5$ and $d_{(201)}$ of NaNbO$_3$, respectively. In Figure 4c, we propose a structural model that depicts the atomic packing in the (210) plane of NaNbO$_3$ and in the (200) plane of Nb$_2$O$_5$ for the multiple heterostructure NaNbO$_3$/Nb$_2$O$_5$ nanotubes. The model suggests that the epitaxial relationships between NaNbO$_3$ nanoplates and Nb$_2$O$_5$ nanotubes are (001)NaNbO$_3$||(001)Nb$_2$O$_5$ and (210)NaNbO$_3$||(200)Nb$_2$O$_5$. Parallel to the nanotube axis, we estimate a relative mismatch of [(0.415–0.394)/0.394 × 100%] = 0.50%. Perpendicular to the nanotube axis we find that the d-spacing between the (210) planes of the NaNbO$_3$ nanoplate is 0.175 nm, and 0.31 nm between the (200) Nb$_2$O$_5$ planes. Therefore, there is a significant apparent mismatch in the heterostructure between the pseudo-cubic perovskite structure NaNbO$_3$ nanoplates and the orthorhombic lattice of the Nb$_2$O$_5$ nanotubes.

Orthorhombic Nb$_2$O$_5$ has a space group of *Pbam* and contains layers of distorted octahedral and pentagonal bipyramids.[25] One out of seventeen Nb atoms occupies the interstitial sites between two unit cells and is surrounded by eight oxygen atoms. These polyhedra are joined by corner or edge sharing in the *ab*-plane and by corner sharing along the *c*-axis. When these polyhedral crystals form tubular structures, the inner surface oxygen atoms of Nb$_2$O$_5$ nanotubes will be closer than those on the outer surface (see the Supporting Information), which results in a larger overlap of electron clouds[26,27] and thus an increased shielding of Nb^{5+} in the center of the polyhedra. This will yield stronger binding of Na$^+$ on the inner surface or more protonated surface sites. In addition, since the Nb$_2$O$_5$ nanotubes have open ends, the inner surface is accessible, and thus the incorporation of species inside the tubes is feasible. Therefore, the preferential growth of multiple NaNbO$_3$ nanoplates on the inner surface of the Nb$_2$O$_5$ nanotubes is related to surface charge polarity developed on outer and inner surfaces due to the difference in overlap of oxygen anions that resulted from the curving of polyhedral structure in the formation process of nanotube structures.

In the growth of the multiple heterostructure NaNbO$_3$/Nb$_2$O$_5$ nanotubes, the initially formed Nb$_2$O$_5$ nanotubes acted as the host in which Nb ions occupy their cation-deficient sites. A charge imbalance between the inner and outer surface of nanotubes could promote strong bonding of the Na ions on the inner wall of Nb$_2$O$_5$. During the ongoing reaction, the NaNbO$_3$ phase starts to nucleate and grows preferentially on the inner surface of the Nb$_2$O$_5$ nanotubes. Further, long-range electrostatic repulsive interaction drives the spontaneous spatial ordering of NaNbO$_3$ nanoparticles inside the nanotubes.[28] At the last stage, the growth of NaNbO$_3$ nanoplates supported by a slow fluoride ion-corrosion of Nb foil leads to the formation of well-aligned nanoplates on the inner surface of nanotubes. The above-proposed growth scenario was verified by interrupting the formation process at different intermediate stages (see the Supporting Information).

To address the functionality of the new multiple heterostructure nanotubes, we first investigated their ferroelectric responses, using piezoresponse force microscopy (PFM, see Fig. 5a).[29,30] As-prepared samples were dispersed in acetone and spread on a surface of a Pt film to produce individually lying heterostructure nanotubes with a diameter of around 500 nm and
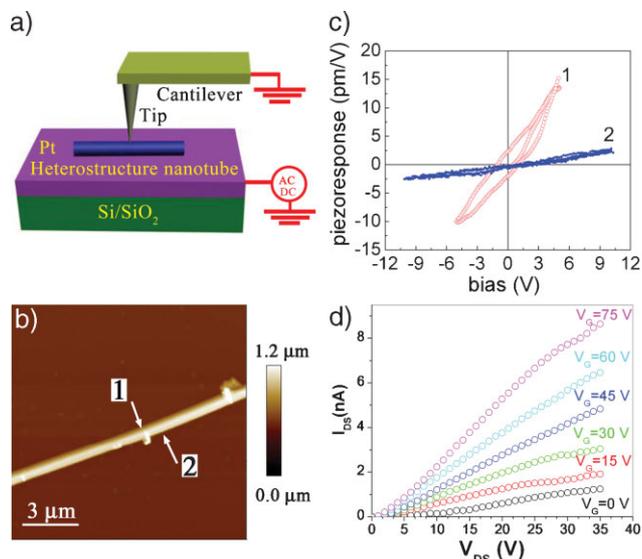
Figure 5. a) Schematic diagram of the PFM experiment. b) PFM image of a single multiple heterostructure $NaNbO_3/Nb_2O_5$ nanotube. c) Representative hysteresis loops from regions indicated in (b) recorded with the tip kept immobile, in contact with a $NaNbO_3$ nanoplate (location "1") and on top of the Nb_2O_5 nanotube (location "2"). d) Output characteristics of multiple $NaNbO_3/Nb_2O_5$ heterostructure nanotubes suspended in ethanol and spin-coated onto SiO_2/Si substrates prepatterned with Au source and drain electrodes ($W/L = 1880/6$ ($\mu m/\mu m$)), where L is the channel length and W is the channel width).

several outgrowths that are used as markers for $NaNbO_3$ nanoplates (Fig. 5b). By positioning the AFM tip on top of a $NaNbO_3$ nanoplate (location "1") we obtain a clear hysteretic behavior characteristic of a ferroelectric state (curve "1" in Fig. 5c). In contrast, positioning the tip on the Nb_2O_5 nanotube at a position free of $NaNbO_3$ nanoplates results in a linear behavior only (curve "2"). According to the $NaNbO_3$ crystal structure at room temperature (orthorhombic space group, *Pbma*, taking into account the atomic shifts), bulk $NaNbO_3$ fulfills the criteria for antiferroelectricity[31] and thus should not exhibit any remnant polarization in zero electric field. The observed ferroelectric behavior can be explained as follows: the $NaNbO_3$ structural changes that take place at the transition between the ferroelectric and antiferroelectric phases are so large that they may cause a huge thermal hysteresis reaching 100–150 °C.[32] This hysteresis was found to depend on the domain twinning in the crystal and it was concluded that stress may play a crucial role in this phase transition.[31] Most likely the piezoelectric switching behavior of $NaNbO_3$ should be somewhat different for each heterostructure with different periodicity, as a result of the difference in stress. Both experimental and theoretical[33] studies indicated that when the characteristic size of a ferroelectric perovskite oxide decreases down to the nanometer scale, even a single lattice defect can control ferroelectric properties. In our case, the $NaNbO_3$ nanoplates grow epitaxially inside the Nb_2O_5 nanotube's walls. According to HR-TEM measurements, the mismatch between the Nb_2O_5 nanotube and the $NaNbO_3$ nanoplate is ~5%, tensile for $NaNbO_3$. For the interface layer under this tensile stress an asymmetrical dislocation leads to expansion of the atoms located

in the $NaNbO_3$ lattice. Since the unit-cell volume in the ferroelectric phase is larger than that of the antiferroelectric phase (where certain Na–O bonds are compressed), a tensile stress will favor the ferroelectric phase, the net effect being a drastic increase of the transition temperature, very likely above room temperature. In addition, it is well known that for certain modified lead zirconate titanate (PZT) antiferroelectric compounds, with compositions close to the antiferroelectric/ferroelectric phase boundary, the application of an electric field can induce a transition to the ferroelectric phase.[34,35] The ferroelectric phase was found to be stable, persisting even after the removal of the electric field. Thus, the electric field applied during the hysteresis measurement could favor the transition to the ferroelectric phase of the $NaNbO_3$, at a very local scale, directly below the AFM tip.

To study the electronic properties of our multiple heterostructured nanotubes, we deposited them on a n-Si/SiO$_2$ substrate and gold electrodes were patterned on top by vacuum evaporation to conduct electrical measurements in field-effect transistor (FET) configuration. A plot of the output characteristics of these devices is shown in Figure 5d. The device is observed to operate in electron-accumulation mode when different positive bias was applied to the gate electrode. It is remarkable that the heterostructure nanotubes function as semiconductors in field-effect transistors even though ferroelectric nanoplates are attached to the inner surface of nanotubes. The presence of ferroelectric $NaNbO_3$ nanoplates in semiconducting Nb_2O_5 nanotubes might affect the intensity of the current devices. This is due to the polarization of $NaNbO_3$, which essentially modifies the electric field distribution and thus the conduction in the heterostructure nanotubes and/or to charge traps at the $NaNbO_3/Nb_2O_5$ interface. However, it is shown that the output curves still exhibit a pinch-off and current saturation behavior, indicating that the operation of the device conforms to standard FET theory and the Fermi level[36,37] in the channel is effectively controlled by the gate and drain bias. These results clearly demonstrate that we can achieve both ferroelectric switching and semiconductor properties in multiple $NaNbO_3/Nb_2O_5$ heterostructure nanotubes, opening the possibility of realizing the integration of ferroelectric materials into semiconductor technology for future multifunctional device purposes.

In summary, we have demonstrated that multiple $NaNbO_3$ nanoplates can be successfully created within Nb_2O_5 nanotubes to form a unique class of multiple heterostructures combining ferroelectric and semiconducting nanomaterials by employing a nanotube-confined growth strategy. The preferential growth of multiple $NaNbO_3$ nanoplates on the inner surface of the Nb_2O_5 nanotubes is related to the electrical polarity developed between the inner and outer surfaces, the confinement effect of nanotubes, and the long-range dipole–dipole interaction. Local piezoelectric studies on $NaNbO_3$ nanoplates show clear ferroelectric behavior, while the semiconducting properties of the host Nb_2O_5 nanotubes allows for efficient switching of electrical conductivity shown by FET studies. Such combination of ferroelectric/semiconducting properties within a single nanomaterial establishes the basis for applications in nanometer-scale memories and other nanoelectronic devices. This work will also open new opportunities for producing multiple heterostructures by employing the nanotube-confined growth method.

Experimental

Preparation: Nb_2O_5 (1.125 g) powder was dissolved in HF (48%) solution in a sealed plastic beaker after heating in a hot oil bath at 140 °C for 8 h. Subsequently, H_2O_2 (30 mL) and $NH_4 \cdot H_2O$ (25% aqueous solution, 10 mL) were added into the above solution to form Nb peroxo complex precursors of general formula $[Nb(O_2)_4]^{3-}$. After that, NaCl (0.3 g) and Na_2SO_4 (1.2 g) were added into the reaction solution followed by adding poly(N-vinyl-2-pyrrolidone) (0.6 g). Finally, the resulting mixture was transferred into a Teflon-line steel autoclave containing a piece of precleaned niobium foil (ca. 1.5 g). The autoclave was then heated at 180 °C for 16 h. The temperature control is very important and other nanostructures (nanorods or nanowires) have been observed to form at temperatures deviation of more than ±20 °C (see the Supporting Information). After cooling down to room temperature, the product was filtered and washed with deionized water and absolute ethanol several times. Finally, the as-prepared sample was calcinated at 600 °C in air to remove the residual polymer.

Characterization: The as-prepared samples were characterized by XRD on a Bruker X-ray diffractometer equipped with graphite monochromatized Cu Kα radiation flux. The structures of multiple heterostructure NaNbO_3/Nb_2O_5 nanotubes and Nb_2O_5 nanotubes were investigated by TEM (Philips CM200 200 kV and JEOL JEM-2100F 200kV) and field-emission SEM (Hitachi S-4700). XPS spectra were obtained with an ESCALAB 220I-XL spectrometer equipped with an Al Kα (1486.6 eV) monochromatic source at base pressures less than 10^{-8} Torr with a perpendicular take-off angle.

Ferroelectric Property Investigation: The ferroelectric properties of NaNbO_3 nanoplates grown inside the Nb_2O_5 nanotubes was investigated using the experimental setup described earlier [29,30]: an Enviroscope atomic force microscope (Veeco) equipped with Ti/Pt-coated NSC36 tips from Mikromasch. We used medium-stiff cantilevers (k ∼ 0.65 N m⁻¹) to achieve a firm contact between tip and nanotube, the contact force during the measurements was 52 nN. We used the non-contact mode of operation for localizing the nanotube. Upon positioning the tip above the selected location on the nanotube, we stopped the lateral scanning and switched to contact mode. We applied 0.5 V at 27 kHz alternating current (AC) excitation and the resulting piezoelectric deformations transmitted to the cantilever were detected from the global deflection signal using a lock-in amplifier (Signal Recovery, model 7265). The large bias required for hysteresis measurements was applied using a DC source (Keithley 2400 Sourcemeter) in series with the AC driving voltage.

Electric Property Investigation: The current–voltage (I–V) characteristics of the FET devices were measured with a Keithley Model-4200 semiconductor characterization system. The nanotube films were deposited on 190-nm-thick SiO_2 thermally grown on heavily n-doped (Sb) Si (ρ ∼ 0.01–0.02 Ohm-cm, ρ is the resistivity in Ohm-cm) and circular Au source/drain electrodes were patterned on top by vacuum evaporation to conduct electrical measurements in FET configuration. Prior to deposition, substrates were cleaned by sonication in acetone and isopropyl alcohol followed by exposure to O_2 plasma.

Acknowledgements

[1] D. Seo, C. Yoo, J. Jung, H. Song, *J. Am. Chem. Soc.* **2008**, *130*, 2940.

[2] R. D. Robinson, B. Sadtler, D. O. Demchenko, C. K. Erdonmez, L. W. Wang, A. P. Alivisatos, *Science* **2007**, *317*, 355.

[3] M. S. Gudiksen, L. J. Lauhon, J. F. Wang, D. C. Smith, C. M. Lieber, *Nature* **2002**, *415*, 617.

[4] B. Yoo, F. Xiao, K. N. Bozhilov, J. Herman, M. A. Ryan, N. V. Myung, *Adv. Mater.* **2007**, *19*, 296.

[5] S. Y. Hong, R. Popovitz-Biro, Y. Prior, R. Tenne, *J. Am. Chem. Soc.* **2003**, *125*, 10470.

[6] R. Kreizman, S. Y. Hong, J. Sloan, R. Popovitz-Biro, A. Albu-Yaron, G. Tobias, B. Ballesteros, B. G. Davis, M. L. H. Green, R. Tenne, *Angew. Chem. Int. Ed.* **2009**, *48*, 1230.

[7] R. R. Meyer, J. Sloan, R. E. Dunin-Borkowski, A. I. Kirkland, M. C. Novotny, S. R. Bailey, J. L. Hutchison, M. L. H. Green, *Science*, **2000**, *289*, 1324.

[8] F. Xue, G. Fei, B. Wu, *J. Am. Chem. Soc.* **2005**, *127*, 15348.

[9] L. Ouyang, K. N. Maher, C. L. Yu, J. McCarty, H. Park, *J. Am. Chem. Soc.* **2007**, *129*, 133.

[10] Y. Wu, R. Fan, P. Yang, *Nano Lett.* **2002**, *2*, 83.

[11] H. Zheng, J. Wang, S. E. Lofland, Z. Ma, L. Mohaddes-Ardabili, T. Zhao, L. Salamanca-Riba, S. R. Shinde, S. B. Ogale, F. Bai, D. Viehland, Y. Jia, D. G. Schlom, M. Wutting, A. Roytburd, R. Ramesh, *Science* **2004**, *303*, 661.

[12] V. Nagarajan, C. L. Jia, H. Kohlstedt, R. Waser, I. B. Misirlioglu, S. P. Alpay, R. Ramesh, *Appl. Phys. Lett.* **2005**, *86*, 192910.

[13] M. Alexe, G. Kastner, D. Hesse, U. Gosele, *Appl. Phys. Lett.* **1997**, *70*, 3416.

[14] T. Mokari, C. G. Sztrum, A. Salant, E. Rabani, U. Banin, *Nat. Mater.* **2005**, *4*, 855.

[15] F. Richter, H. Kupfer, P. Schlott, T. Gessner, C. Kaufmann, *Thin Solid Films* **2001**, *389*, 278.

[16] D. F. Perepichka, F. Rosei, *Small* **2006**, *2*, 22.

[17] B. Li, L. Li, B. Wang, C. Y. Li, *Nat. Nanotechnol.* **2009**, *4*, 358.

[18] L. Margulis, G. Salitra, R. Tenne, M. Tallanker, *Nature* **1993**, *365*, 113.

[19] Y. R. Hacohen, E. Grunbaum, R. Tenne, J. Sloan, J. L. Hutchison, *Nature* **1998**, *395*, 336.

[20] R. Tenne, L. Margulis, M. Genut, G. Hodes, *Nature* **1992**, *360*, 444.

[21] D. Bayot, B. Tinant, M. Devillers, *Catal. Today* **2003**, *78*, 439.

[22] T. Saito, T. Wada, H. Adachi, I. Kanno, *Jpn. J. Appl. Phys.* **2004**, *43*, 6627.

[23] D. Morris, Y. Dou, J. Rebane, C. E. J. Mitchell, R. G. Egdell, D. S. Law, A. Vittadini, M. Casarin, *Phys. Rev. B* **2000**, *61*, 13445.

[24] J. Kubacki, A. Molak, E. Talik, *J. Alloys Compd.* **2001**, *328*, 156.

[25] C. Yan, D. Xue, *Adv. Mater.* **2008**, *20*, 1055.

[26] H. Xu, G. Vanamu, Z. Nie, H. Konishi, R. Yeredla, J. Phillips, Y. Wang, *J. Nanomater.* **2006**, DOI: 10.1155/JNM/2006/78902.

[27] W. H. Van Riemsdijk, J. C. M. De Wit, L. K. Koopal, G. H. Bolt, *J. Colloid Interface Sci.* **1987**, *116*, 511.

[28] Z. Tang, N. A. Kotov, M. Giersig, *Science* **2002**, *297*, 237.

[29] C. Harnagea, C. V. Cojocaru, R. Nechache, O. Gautreau, F. Rosei, A. Pignolet, *Int. J. Nanotechnol.* **2008**, *5*, 930.

[30] C. Harnagea, A. Pignolet, M. Alexe, D. Hesse, *IEEE Trans. Ultrason. Ferroelect. Freq. Control* **2006**, *53*, 2309.

[31] C. N. W. Darlington, H. D. Megaw, *Acta Cryst. B* **1973**, *29*, 2171.

[32] L. E. Cross, B. J. Nicholson, *Phil. Mag.* **1955**, *46*, 453.

[33] C. L. Jia, S. B. Mi, K. Urban, I. Vrejoiu, M. Alexe, D. Hesse, *Phys. Rev. Lett.* **2009**, *102*, 117601.

[34] K. Y. Oh, Y. Saito, A. Furuta, K. Uchino, *J. Am. Ceram. Soc.* **1992**, *75*, 795.

[35] R. E. Koritala, M. T. Lanagan, N. Chen, G. R. Bai, Y. Huang, S. K. Streiffer, *J. Mater. Res.* **2000**, *15*, 1962.

[36] J. S. Blakemore, *Solid-State Physics*, 2nd ed. Cambridge University Press, Cambridge, UK **1985**, pp. 202–204.

[37] C. Santato, F. Cicoira, P. Cosseddu, A. Bonfiglio, P. Bellutti, M. Muccini, R. Zamboni, F. Rosei, A. Mantoux, P. Doppelt, *Appl. Phys. Lett* **2006**, *88*, 163511.